Optics Letters

Spectral singularities and asymmetric light scattering in PT-symmetric 2D nanoantenna arrays

JINAL TAPAR, SAURABH KISHEN, AND NARESH KUMAR EMANI*

Department of Electrical Engineering, Indian Institute of Technology, Hyderabad 502285, India
**Corresponding author: naresh@ee.iith.ac.in*

Received 26 May 2020; revised 3 August 2020; accepted 3 August 2020; posted 4 August 2020 (Doc. ID 398551); published 14 September 2020

The intriguing physics of non-Hermitian systems satisfying parity-time (PT) symmetry has spurred a surge of both theoretical and experimental research in interleaved gain-loss systems for novel photonic devices. In this work, we investigate vertically stacked GaInP PT-symmetric nanodisk resonators arranged in two-dimensional periodic lattice using full-wave numerical simulations and scattering matrix theory. The proposed dielectric metasurface supports lasing spectral singularities with asymmetric reflection and highly anisotropic far-field scattering patterns. It offers a much broader design parameter space to control wavelength, scattering direction, and efficiency of optical emission when compared to the predominantly one-dimentional (1D) or quasi-1D structures studied so far. The proposed system with Q-factor $>10^5$ serves as a powerful platform for enhanced light-matter interaction by enabling extensive control of asymmetric light scattering, amplification, and unprecedented localization of electromagnetic fields.

https://doi.org/10.1364/OL.398551

Fundamental postulates of quantum mechanics dictate that a closed system must be described by Hermitian Hamiltonians to guarantee real eigenvalues and a complete set of eigenvectors. The existence of real eigenvalues for non-Hermitian Hamiltonians obeying PT (parity-time) symmetry [1] has triggered an exploration of a wide range of experiments to study counter-intuitive dynamics such as single-mode lasing [2], unidirectional invisibility [3], coherent perfect absorber (CPA)-laser [4], and non-reciprocal [5] and anisotropic transmission resonance [6]. In the context of photonics, PT-symmetry [7,8] implies that the complex refractive index profile must be of the form $n(\mathbf{r}) = n^*(-\mathbf{r})$, implying the real and imaginary parts of the refractive index have to be even and odd functions of the spatial coordinate $\mathbf{r}$, respectively. The interplay of gain-loss contrast, i.e., the non-Hermiticity factor, and the coupling in PT-symmetric systems has resulted in several exciting breakthroughs, especially near the PT-phase transition points. A common and widely explored mechanism of the transition of non-Hermitian systems from the PT-symmetric phase (real eigenvalues) to broken-PT phase (complex conjugate pair of eigenvalues) is through the occurrence of exceptional points (EPs) [9–12]. These EPs correspond to degeneracy in the *discrete spectrum* of a non-Hermitian Hamiltonian operator, where both eigenvalues and eigenvectors coalesce as the system parameters (gain-loss contrast or coupling) are varied. Another mechanism by which PT-symmetric systems can undergo PT-phase transition is through the emergence of spectral singularities (SS) [13]. The SS are the points in the *continuous spectrum* of a non-Hermitian Hamiltonian operator, where the scattering coefficients tend to infinity [14]. A necessary and sufficient condition for a given non-Hermitian potential to support SS at a prescribed wavelength is discussed in [15]. Theoretically, it has been shown that SS in the PT-symmetric system are self-dual, i.e., they can behave simultaneously as a laser oscillator and as a CPA [16–18]. In contrast to EPs and CPA points that can be realized in passive configurations, lasing SS can occur only in the presence of gain [19]. The SS, being poles of the scattering matrix at real frequencies, imply zero-width resonances and have applications like super scattering, nanolasers, and other non-linear phenomena where strong light-matter interaction is desired.

The exact condition of PT-symmetry can be satisfied only at isolated frequency points [20] for gain/loss materials exhibiting a Lorentzian line-shape spectrum. However, the concept of quasi-PT symmetry [21] allows the PT-symmetry conditions to be achieved over a finite frequency range. Active solid-state materials like III-V semiconductors are suitable candidates for designing quasi-PT symmetric optical devices due to their broad gain spectrum. Previously, research in the context of EPs and SS has focused on micron-scale photonic structures incorporating gain-loss balance or passive PT-symmetry. When the systems are scaled into the nanoscale dimensions, the losses become significant and requirements on gain become stringent. In this work, we propose an active two-dimensional GaInP metasurface operating at optical wavelengths. The proposed metasurface exhibits tunable SS whose wavelength, amplitude, and scattering response can be efficiently tuned by both geometry and gain (optical pumping). The simulated structure consists of a two-dimensional (2D), PT-symmetric metasurface of vertically coupled GaInP disks separated by an SiO_2 spacer, as shown

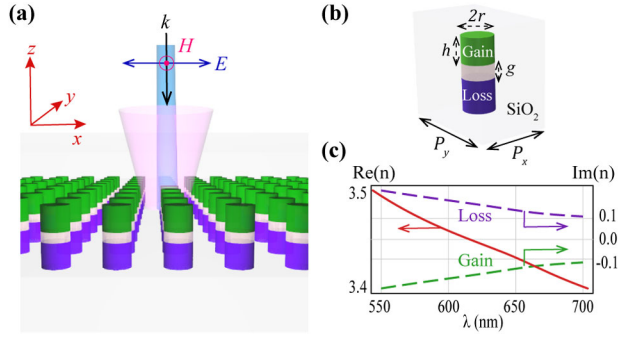

Fig. 1. (a) Schematic illustration of the PT-symmetric GaInP metasurface with TM polarized light (E-field along the x-axis at normal incidence); gain-loss modulation is along the z-axis, parallel to incident wave vector k. (b) Unit cell consisting of a rectangular lattice with sub-diffractive periodicity $P_x = 400$ nm along the x-axis and diffractive periodicity $P_y = 550$ nm along the y-axis. The radius ($r = 100$ nm) and height ($h = 250$ nm) of each GaInP nanodisk are varied to overlap the collective resonance of the array with the gain spectrum of GaInP. Varying the spacer gap g determines the coupling between gain and loss resonator, and thereby the phase of PT-symmetry. The overall structure is embedded in SiO_2 to create a homogenous environment. (c) The refractive index exhibits dispersion of the form $n(\lambda, z) = n^*(\lambda, -z)$ such that it satisfies the quasi-PT-symmetry condition.

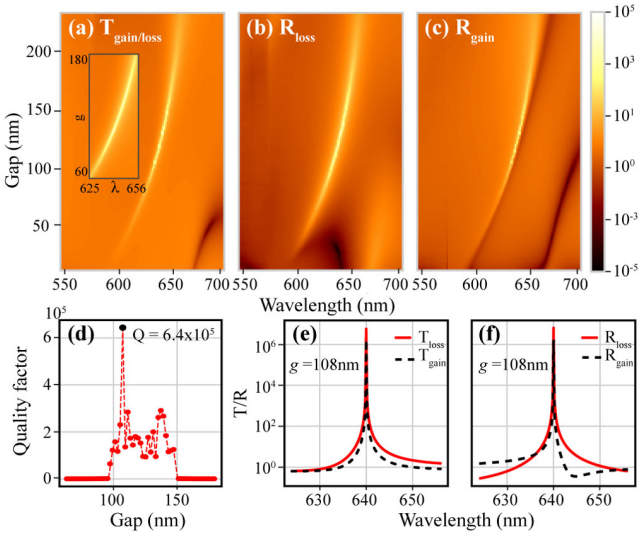

Fig. 2. Emergence of SS with the varying gap between the resonators can be observed in (a) transmission, which is identical for illumination from both the gain and the loss side, and reflection for illumination from (b) loss and (c) gain sides, which shows asymmetric behavior. Inset in (a) shows the spectra with a finer sweep of the gap. SS are tunable and red-shift with the increasing gap (reduced coupling) between the gain-loss resonators. (d) Quality factor of the system with varying gap g between the resonators. On the emergence of SS, the Q-factor rises sharply with the highest value, $Q = 6.4 \times 10^5$ at $\lambda = 640$ nm and $g = 108$ nm. The Q-factor value in the range $g = 100-150$ nm varies with an average $Q \sim 1.5 \times 10^5$ over the range. (e) Transmission and (f) reflection spectra diverge at the SS and resemble a zero-width resonance.

in Fig. 1. The gain-loss modulation is introduced along the z-direction, longitudinal to the wave propagation direction. The coupling between the disks is determined by the thickness (g) of the SiO_2 spacer layer, and the structure is embedded in SiO_2 to provide a homogeneous environment.

The geometric parameters (radius r and height h) of the resonators and the lattice periodicities (P_x and P_y) are tuned to overlap the SS with the PL (photoluminescence spectrum) of GaInP (FWHM $\Delta\lambda = 630-670$ nm with a peak at $\lambda = 655$ nm). We consider the refractive index profile for GaInP meta-atom with dispersion in the wavelength range of $\sim$550$-$700 nm, as in Fig. 1(c). The proposed GaInP metasurface can be realized experimentally by judiciously adjusting the doping level and thereby gain [22] in the GaInP semiconductor. The structure is studied numerically by carrying out full-wave three-dimensional (3D) simulations in FEM (Finite Element Method) software (COMSOL Multiphysics, Stockholm, Sweden). The simulation domain consists of a rectangular unit cell of the array with periodic Bloch boundary conditions along x and y directions. The stacked nanopillar representing the PT-symmetric GaInP resonator is excited using port boundary conditions at the top and bottom of the unit cell. The incident light is normal to the metasurface (along the z-axis), and the electric field is polarized along the x-axis. We refer to the scattered power in the forward direction as transmission and the scattered power in the backward direction as reflection. The scattered power in various diffraction orders supported by the lattice is calculated by using appropriate port conditions in both transmission and reflection.

Figures 2(a)–2(c) show the calculated transmission and reflection for p-polarized light passing through the PT-symmetric GaInP nanodisk array as a function of the wavelength and the gap parameter (g). The transmission is identical for illumination from either gain or loss side, but the reflection shows an asymmetric response. The asymmetry in reflection is due to the different positions of the gain and loss regions relative to the illumination ports. However, this does not violate the Lorentz reciprocity condition as the system is linear and non-magnetic. For smaller gaps ($g < 60$ nm in this case), the structure is in the PT-symmetric phase, i.e., balanced gain-loss, and hence no SS are present.

For $g > 60$ nm, we see a strong divergence in the reflection and transmission profile. As the gap increases, the effective time-reversal symmetry breaking perturbation gets stronger, and the metamaterial enters the PT-broken phase [23]. In the broken PT-phase, for a finite range of wavelength, photons spend more time in the gain nanodisk compared to the loss nanodisk, leading to a net gain in the system. This results in the emergence of SS. From Figs. 2(a)–2(c), we can see that the SS gradually shifting to longer wavelengths with the increasing gap, i.e., reduced coupling. The SS in the proposed metasurface show continuous evolution along the wavelength axis over a wide range of gap. The observed broad spectral tunability of SS can be attributed to the presence of multiple degrees of freedom in the proposed metasurface. Like bound states in the continuum (BIC), the SS lead to extremely large Q-factors at the wavelength at which they occur, as seen in Fig. 2(d). The highest value of the Q-factor is observed at $g = 108$ nm, and the corresponding transmission and reflection spectra are plotted in Figs. 2(e) and 2(f), respectively. Note that the transmission for incidence from either side seems to be asymmetric in the vicinity of SS due to the finite numerical resolution of the simulation tool. The varying Q-factor with an average value of $\sim 1.5-2 \times 10^5$ over a range

of gap parameter ($g = 100$ to 150 nm) provides flexibility to control the wavelength-selective efficiency of optical emission in the proposed structure.

To further understand the observed divergence of transmission/reflection coefficients in the proposed PT-symmetric metasurface, we analyze the zeros of its transfer matrix. In a 1D scattering with two ports, the amplitudes of forward and backward propagating waves on either side of the system are related to each other by a 2×2 transfer matrix given as $M = \begin{pmatrix} M_{11} & M_{12} \\ M_{21} & M_{22} \end{pmatrix}$ [24]. In a linear 1D scattering system, the SS are the real zeros of $M_{22}(\omega)$, i.e., at SS, the relation $M_{22}(\omega_{ss}) = 0$ is satisfied [25]. However, as seen in Fig. 3(a), the proposed vertically coupled PT metasurface with the lattice periodicities of $P_x = 400$ nm and $P_y = 550$ nm supports zeroth and first diffraction orders for incident light in the wavelength range ~500−800 nm. To examine how the relation $M_{22}(\omega) = 0$ is satisfied in the 2D metasurface with more than two channels, we constructed a 6×6 dimensional transfer matrix for the proposed system using the scattering matrix approach (section 2 of [26]). First, the 6×6 S-matrix was constructed by computing the scattered power in the three channels, each on either side of the structure for normal incidence. The S-matrix elements were obtained by performing several simulations by setting $A_l^+ = 1$ ($A_g^- = 1$) for incidence from loss (gain) side. This computed S-matrix was transformed into a 6×6 transfer matrix, as shown in (1), using the canonical interchangeability relation between 2×2 matrix elements of scattering and transfer matrices [24]

$$\begin{pmatrix} a_g^+ \\ A_g^- \\ b_g^+ \\ A_g^- \\ c_g^+ \\ A_g^- \end{pmatrix} = \begin{pmatrix} M_{11} & M_{12} & 0 & 0 & 0 & 0 \\ M_{21} & M_{22} & 0 & 0 & 0 & 0 \\ 0 & 0 & M_{33} & M_{34} & 0 & 0 \\ 0 & 0 & M_{43} & M_{44} & 0 & 0 \\ 0 & 0 & 0 & 0 & M_{55} & M_{56} \\ 0 & 0 & 0 & 0 & M_{65} & M_{66} \end{pmatrix} \begin{pmatrix} A_l^+ \\ a_l^- \\ A_l^+ \\ b_l^- \\ A_l^+ \\ c_l^- \end{pmatrix}. \quad (1)$$

The first block matrix (M_{11} to M_{22}) corresponds to the zeroth diffraction order and remaining block matrices (M_{33} to M_{44}) and (M_{55} to M_{66}) corresponds to -1st and 1st order, respectively. The magnitude of terms M_{22}, M_{44}, and M_{66} (equivalent M_{22} terms for each diffraction order) are plotted in Figs. 3(b)–3(d), whereas their sum is plotted in Fig. 3(e). It is evident from Fig. 3(e) that the occurrence of SS in the proposed system is accompanied by the equivalent M_{22} terms for the allowed diffraction channels going to zero. The magnitude of equivalent M_{22} terms along cut lines (1) and (2) in Fig. 3(e), for the varying gap at $\lambda = 640$ nm and varying wavelengths at $g = 108$ nm, is plotted to show the contribution of the equivalent M_{22} terms at the SS. Thus, in the proposed PT-symmetric metasurface, the equivalent M_{22} terms going to zero at SS implies the amplification of scattered power in all the allowed channels.

The SS in the proposed structure exhibits an interesting directional response. One of the earlier works on a PT-symmetric plasmonic dimer [27] reported the scattering of light predominantly towards the gain side of the structure, while another work on a PT-symmetric Janus cylinder [28] stated that the deflection of light is towards the loss sector irrespective of illumination direction. We show that the anisotropic directional response of

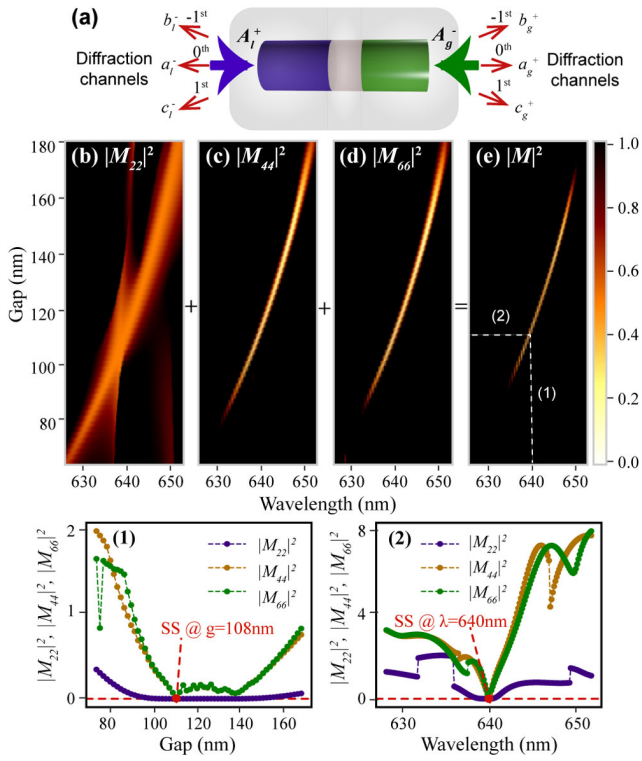

Fig. 3. (a) For the given lattice periodicities, our structure supports zeroth and 1st order outgoing, diffraction channels shown by the red arrows. Two incoming channels from each side are denoted by bold arrows. The amplitude coefficients (indicated by a for 0th, and b, c for -1st, 1st order) are subscripted with l and g for the loss and the gain sides, respectively. (b)–(d) The magnitude of $|M_{22}|^2$, $|M_{44}|^2$ and $|M_{66}|^2$ terms of the transfer matrix corresponding to zeroth and -1st and 1st diffraction channels supported by the proposed metamaterial highlighting their corresponding zeros. (e) Addition of terms in (b)–(d) leading to absolute zeros → $|M_{22}| = 0$ at the wavelength of SS. The magnitude of equivalent M_{22} terms along cut lines (1) and (2) is plotted.

SS in our proposed PT-symmetric nanoantenna array can be tuned to show predominant scattering towards either side of the structure, thus enabling the directionality control. As shown in Fig. 4(a) for lattice periodicities of $P_x = 400$ nm, $P_y = 550$ nm (one sub-diffractive and one diffractive), the far-field scattering of the E-field is directed towards the loss side irrespective of the excitation port. Figure 4(b) plots the ratio of forward to backward (F/B) scattered intensities showing that backscattering is dominant when light is incident from the loss side, and forward scattering dominant when light is incident from the gain side. Further, the magnitude of the E-field is much stronger in the case of excitation from the loss side. On the contrary, Figs. 4(c) and 4(d) plot the scattering profile and F/B ratio for the case of sub-diffractive periodicities ($P_x = 300$ nm, $P_y = 350$ nm) along both the axes with SS appearing at a longer wavelength $\lambda = 691$ nm. Here, irrespective of the direction of the illumination, the far-field scattering is dominant towards the gain side. With gain-side illumination, the backscattering is dominant with a larger magnitude while forward scattering dominates for illumination from the loss-side. We believe that the complex interference of the magneto-electric resonances and lattice modes excited in each PT-symmetric nanoantenna

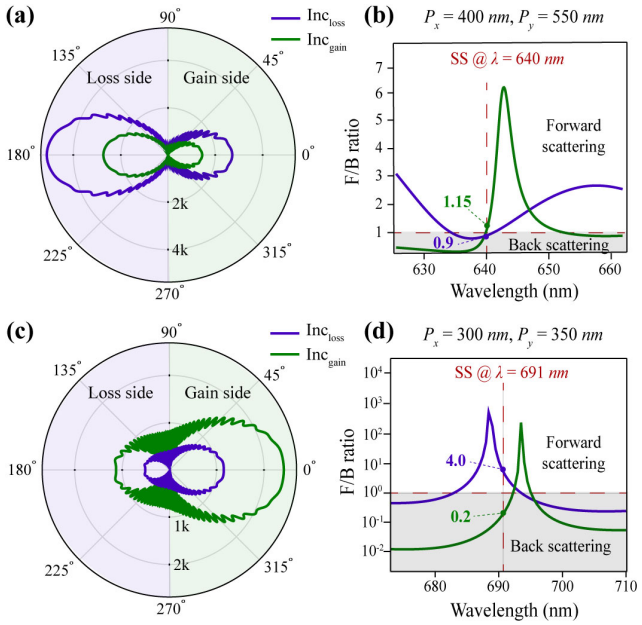

Fig. 4. (a) At the SS wavelength, the scattering lobe is dominant towards the loss side irrespective of the excitation direction. It is more prominent in the case of excitation from the loss side compared to the gain side. (b) The F/B ratio shows backscattering to be dominant for incidence from the loss side, while forward scattering is dominant when light is incident from the gain side at SS. (c) For PT-metamaterial with both sub-diffractive periodicities ($P_x = 300$ nm, $P_y = 350$ nm), the scattering lobe is dominant towards the gain side irrespective of the illumination side with a higher magnitude when light is incident from the gain side at SS, $\lambda = 691$ nm. (d) The F/B ratio shows backscattering to be dominant for incidence from the gain side while forward scattering is dominant when light is incident from the loss side. The direction and magnitude of asymmetric scattering are dictated by the interplay of Mie resonances at the SS wavelength determined by the gain-loss contrast and coupling between them due to SiO_2 spacer thickness and the unit cell periodicities.

in the array gives rise to conditions similar to Kerker's first and second conditions observed in dielectric nanoantennas [29,30]. The control of the coupling between loss and gain resonators, the interference between their modes, and the overall 2D-lattice resonances will provide a route towards designing a special class of tunable sources exhibiting direction-sensitive emission properties.

From the viewpoint of the experimental realization of the proposed metasurface, we note that the fabrication-induced disorder and the material-related non-idealities are unavoidable. These can cause the extremely narrow-width SS to manifest as finite-width resonances with small detuning from predicted SS wavelengths. The overall Q-factor can also be expected to be less by $\sim 2-3$ orders of a magnitude similar to the results in [30], but still sufficient to observe the effects shown in Figs. 2 and 4.

In conclusion, we demonstrate the existence of SS in an open PT-symmetric nanoresonator scattering system for the visible spectrum. The SS in the proposed structure offers two unique advantages: (i) they are robust to parameter variations and are tunable both in wavelength and amplitude, and (ii) the far-field scattering is highly directional. Our analysis suggests that a proper combination of geometry, gain, and subwavelength resonances provides flexibility for designing tunable and directional nanophotonic light sources employing non-Hermitian physics. The strong localization of the fields at SS and the unusual directional response will be useful in applications where strong light-matter interaction with directionality is desired, such as ultrasensitive sensors, non-reciprocal amplifiers/attenuators, and non-linear devices.

Funding. Science and Engineering Research Board (ECR/2018/002452, SB/S2/RJN-007/2017); Ministry of Human Resource Development (STARS/APR2019/NS/774).

Disclosures. The authors declare no conflicts of interest.

REFERENCES

1. C. M. Bender and S. Boettcher, Phys. Rev. Lett. **80**, 5243 (1998).
2. L. Feng, Z. J. Wong, R.-M. Ma, Y. Wang, and X. Zhang, Science **346**, 972 (2014).
3. L. Feng, Y.-L. Xu, W. S. Fegadolli, M.-H. Lu, J. E. Oliveira, V. R. Almeida, Y.-F. Chen, and A. Scherer, Nat. Mater. **12**, 108 (2013).
4. Z. J. Wong, Y.-L. Xu, J. Kim, K. O'Brien, Y. Wang, L. Feng, and X. Zhang, Nat. Photonics **10**, 796 (2016).
5. B. Peng, Ş. K. Özdemir, F. Lei, F. Monifi, M. Gianfreda, G. L. Long, S. Fan, F. Nori, C. M. Bender, and L. Yang, Nat. Phys. **10**, 394 (2014).
6. L. Ge, Y. Chong, and A. D. Stone, Phys. Rev. A **85**, 023802 (2012).
7. R. El-Ganainy, K. G. Makris, M. Khajavikhan, Z. H. Musslimani, S. Rotter, and D. N. Christodoulides, Nat. Phys. **14**, 11 (2018).
8. S. Longhi, Europhys. Lett. **120**, 64001 (2018).
9. M.-A. Miri and A. Alù, Science **363**, eaar7709 (2019).
10. Ş. Özdemir, S. Rotter, F. Nori, and L. Yang, Nat. Mater. **18**, 783 (2019).
11. W. Heiss, J. Phys. A **45**, 444016 (2012).
12. H. Xu, D. Mason, L. Jiang, and J. Harris, Nature **537**, 80 (2016).
13. V. V. Konotop and D. A. Zezyulin, Opt. Lett. **42**, 5206 (2017).
14. A. Mostafazadeh, Phys. Rev. Lett. **102**, 220402 (2009).
15. V. V. Konotop, E. Lakshtanov, and B. Vainberg, Phys. Rev. A **99**, 043838 (2019).
16. Y. Chong, L. Ge, and A. D. Stone, Phys. Rev. Lett. **106**, 093902 (2011).
17. S. Longhi, Phys. Rev. A **82**, 031801 (2010).
18. Y. Chong, L. Ge, H. Cao, and A. D. Stone, Phys. Rev. Lett. **105**, 053901 (2010).
19. A. Mostafazadeh, Phys. Rev. A **83**, 045801 (2011).
20. A. Zyablovsky, A. Vinogradov, A. Dorofeenko, A. Pukhov, and A. Lisyansky, Phys. Rev. A **89**, 033808 (2014).
21. D. Tsvetkov, V. Bushuev, V. Konotop, and B. Mantsyzov, Phys. Rev. A **98**, 053844 (2018).
22. J. Tapar, S. Kishen, K. Prashant, K. Nayak, and N. K. Emani, J. Appl. Phys. **127**, 153102 (2020).
23. P. Ambichl, K. G. Makris, L. Ge, Y. Chong, A. D. Stone, and S. Rotter, Phys. Rev. X **3**, 041030 (2013).
24. P. Markos and C. M. Soukoulis, *Wave Propagation: From Electrons to Photonic Crystals and Left-Handed Materials* (Princeton University, 2008).
25. A. Mostafazadeh and H. Mehri-Dehnavi, J. Phys. A **42**, 125303 (2009).
26. A. Krasnok, D. Baranov, H. Li, M.-A. Miri, F. Monticone, and A. Alú, Adv. Opt. Photon. **11**, 892 (2019).
27. A. Manjavacas, ACS Photon. **3**, 1301 (2016).
28. M.-A. Miri, M. A. Eftekhar, M. Facao, A. F. Abouraddy, A. Bakry, M. A. Razvi, A. Alshahrie, A. Alù, and D. N. Christodoulides, J. Opt. **18**, 075104 (2016).
29. Y. H. Fu, A. I. Kuznetsov, A. E. Miroshnichenko, Y. F. Yu, and B. Luk'yanchuk, Nat. Commun. **4**, 1527 (2013).
30. S. T. Ha, Y. H. Fu, N. K. Emani, Z. Pan, R. M. Bakker, R. Paniagua-Domínguez, and A. I. Kuznetsov, Nat. Nanotech. **13**, 1042 (2018).